

# Universality of oscillating boiling in Leidenfrost transition

Mohammad Khavari<sup>1,2</sup> and Tuan Tran<sup>1\*</sup>

<sup>1</sup> School of Mechanical & Aerospace Engineering,

Nanyang Technological University, 50 Nanyang Avenue, 639798, Singapore

<sup>2</sup> Institute of Materials Research and Engineering, A\*STAR, 3 Research Link, 117602, Singapore

(Dated: March 13, 2022)

The Leidenfrost transition leads a boiling system to the boiling crisis, a state in which the liquid loses contact with the heated surface due to excessive vapor generation. Here, using experiments of liquid droplets boiling on a heated surface, we report a new phenomenon, termed oscillating boiling, at the Leidenfrost transition. We show that oscillating boiling results from the competition between two effects: separation of liquid from the heated surface due to localized boiling, and rewetting. We argue theoretically that the Leidenfrost transition can be predicted based on its link with the oscillating boiling phenomenon, and verify the prediction experimentally for various liquids.

Boiling of liquid on a moderately heated surface removes heat effectively: the liquid absorbs heat after touching the surface, vaporizes, and the generated vapor is carried away by natural convection, letting liquid from the bulk replenish the surface. At elevated temperatures, this mechanism faces a fundamental problem, the so-called boiling crisis, whereby excessive vapor completely eliminates liquid-surface contact (the Leidenfrost effect), causing a severe drop in heat flux. Controlling occurrence of the Leidenfrost effect therefore is vital to either applications intolerant of the boiling crisis [1], or those taking advantages of the liquid-surface separation [2]. Nonetheless, despite its centuries-old history dating back to 1756 [3], the transition to the Leidenfrost regime remains rich in empirical studies, but incomplete in physical understanding [4].

Research efforts aiming at understanding the Leidenfrost phenomenon have focused on the case of *static* Leidenfrost droplets, i.e., droplets approaching a heated surface with negligible or small initial velocity and subsequently floating on the surface. The floating mechanism in this case has been studied in great details: the viscous flow of vapor between a floating droplet and a heated surface provides a counter force to the droplet's weight [5–8]. Similar hydrodynamical arguments have also been used to explain the bouncing behavior without contact of droplets falling on an unheated smooth surface with small velocity; the counter force in this case is induced by the gas flow [9]. Although these theories have been successfully used to explain the floating mechanism in the static case, they have been assuming *a priori* existence of the gas/vapor layer, thus precluding reference to the contact boiling behavior and its role in the Leidenfrost transition. Their limitation is already hinted by experimental evidences in the case of *dynamic* Leidenfrost droplets [10–12], i.e., those approaching the heated surface with high velocity. In such case, the Leidenfrost transition becomes independent of the impact velocity, signalling another separating mechanism instead of the one based on the gas/vapor flows. As a result, these theories cannot be used to reveal the mechanism of the Lei-

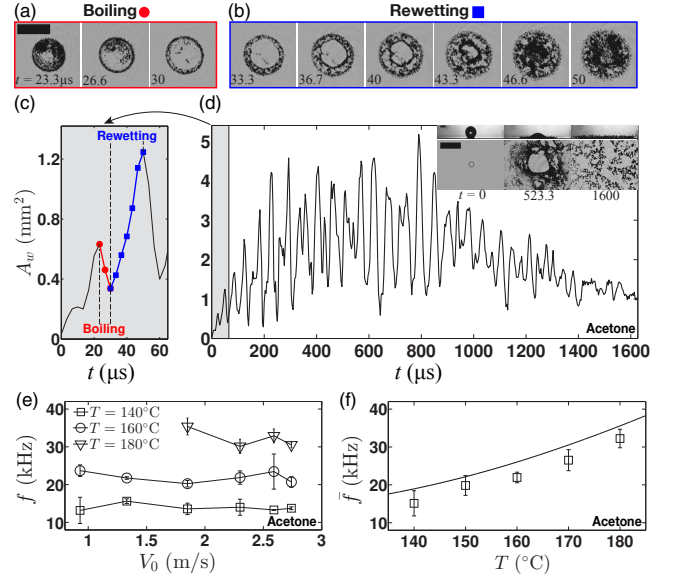


FIG. 1. Snapshots showing the wetted area, measured by the total internal reflection (TIR) technique [11–14], of (a) the boiling process and (b) the rewetting process for acetone droplets with velocity  $V_0 = 2.7 \text{ m} \cdot \text{s}^{-1}$  and surface temperature  $T = 150^\circ \text{C}$ . (c) Wetted area  $A_w$  vs.  $t$  in the early stage of a droplet impacting on a heated sapphire surface. (d) Wetted area  $A_w$  vs.  $t$  during the entire impact process; the shaded area corresponds to the wetted area shown in (c). Inset: snapshots show side-view (upper panel) and bottom-view (lower panel) of the impact at different times. (e) Frequency  $f$  of oscillation vs.  $V_0$  for different values of  $T$  showing a weak dependence of  $f$  on  $V_0$ . (f) Frequency  $\bar{f}$  averaged across  $V_0$  vs.  $T$ . The solid line is the frequency  $V_{\text{re}}/R_d$ , where  $V_{\text{re}}$  is the rewetting velocity (Eqn. 1), and  $R_d \approx 1 \text{ mm}$  the droplet radius. All scale bars indicate the length scale of 1 mm.

denfrost transition. The goal of this paper is to elucidate the Leidenfrost transition experimentally and theoretically.

We show that the boiling behavior at the Leidenfrost transition is dominated by a new phenomenon, namely oscillating boiling. This boiling behavior results from the competition between two effects: separation of liquid from the heated surface due to localized boiling, and

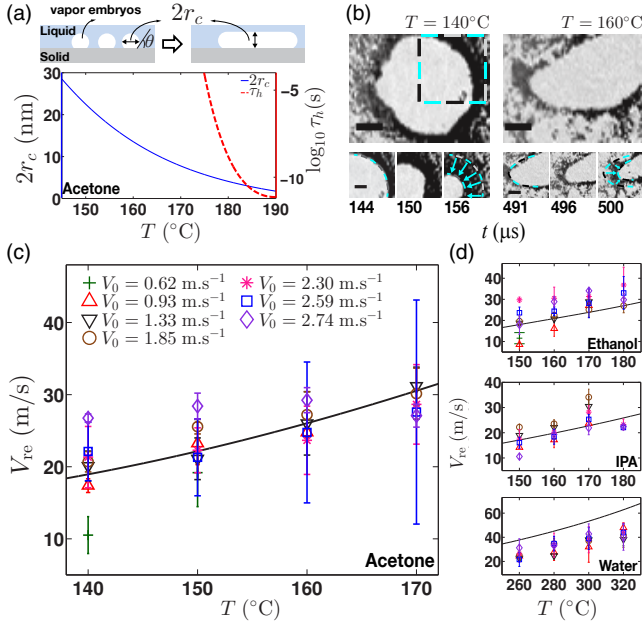


FIG. 2. (a) Critical size  $2r_c$  of a vapor embryo (solid line) and evaporation time  $\tau_h$  (dashed line) versus surface temperature  $T$ . Upper panel: schematic showing vapor embryos before and after merging to create a vapor layer. (b) Snapshots showing the rewetting process for acetone droplets impacting with velocity  $V_0 = 2.3 \text{ m} \cdot \text{s}^{-1}$  at low temperature (left panel) and high temperature (right panel); arrows indicate the motion of the three phase contact line. Scale bars represent the length scale of 0.3 mm. The time stamps are measured from the first contact of impact. (c) Rewetting velocity  $V_{re}$  versus surface temperature  $T$  for acetone droplets for different impact velocities. (d)  $V_{re}$  vs.  $T$  for different impact velocities for ethanol, IPA, and water. Solid lines show the prediction according to Eqn. 1.

rewetting.

To show the oscillating boiling behavior, we visualize the surface's wetted areas and measure the total wetted area  $A_w$  as a function of time  $t$  (Fig. 1). For droplet impacts in a wide range of velocity, liquids (see Table I), and surface temperatures close to the Leidenfrost transition,  $A_w$  oscillates at remarkably high frequencies in the range 12 – 32 kHz (Fig. 1c and d). We observe that the frequency  $f$  of oscillation depends weakly on the impact velocity  $V_0$  (Fig. 1e), but more significantly on the surface temperature  $T$  (Fig. 1f).

The repeating pattern of the total wetted area  $A_w$  typically consists of two distinct stages: an abrupt drop and a subsequent increase in  $A_w$  (Fig. 1c). In the first stage, exemplified in Fig. 1a, tiny dry spots first appear spontaneously and rather uniformly in the wetted area, then expand and merge to create larger dry areas. This observation suggests that the decrease in  $A_w$  is primarily caused by *heterogeneous* boiling, a process of forming the vapor from the liquid on a solid surface at temperatures lower than boiling in liquid (*homogeneous* boiling) [15, 16]. In the second stage, however, the wetted areas merge and invade the dry ones in the direction perpendicular to the

TABLE I. Physical properties of the liquids at  $20^\circ\text{C}$  and atmospheric pressure [29, 33], and experimental conditions.

Unit	Acetone	Ethanol	IPA	Water
$\sigma$ $\text{mN} \cdot \text{m}^{-1}$	23.7	22.8	21.7	72.9
$\rho_l$ $\text{kg} \cdot \text{m}^{-3}$	790	800	781	999
$T_b$ $^\circ\text{C}$	56	78	82	100
$h_{fg}$ $\text{kJ} \cdot \text{kg}^{-1}$	552	1030	755	2454
$C_p$ $\text{kJ} \cdot \text{kg}^{-1} \cdot \text{K}^{-1}$	2.16	2.4	2.6	4.18
$M$ $\text{kg} \cdot \text{kmol}^{-1}$	58.1	46	60.1	18
$R_d$ mm	1.0	1.0	1.0	1.2
$V_0$ $\text{m} \cdot \text{s}^{-1}$	0.6–2.7	0.5–2.7	0.5–2.7	0.5–2.8
$T$ $^\circ\text{C}$	20–370	20–210	20–230	20–520

three-phase contact line, signifying a rewetting process (Fig. 1b). On this basis, we postulate that heterogeneous boiling and rewetting are the two basic processes of the oscillating boiling behavior; the rapid fluctuation of  $A_w$  results from alternate domination of one process over the other (Movies S1-S6).

We now analyze the heterogeneous boiling process. On an ideally flat surface immersed in a liquid at temperature  $T_l$  and pressure  $P_l$ , vapor bubbles grow from embryos, tiny nanoscopic vapor pockets in the form of spherical caps attaching to the surface (Fig. 2a, schematics). For an embryo to grow into a vapor bubble, the pressure difference across the vapor-liquid interface must overcome the Laplace pressure. Equivalently, its radius must be larger than a critical value  $r_c = 2\sigma F / (P_v - P_l)$ , where  $F$  is a correction factor to account for the partial spherical shape of the embryo [20]. Here, the vapor pressure  $P_v$  inside the embryo depends on  $T_l$  and  $P_l$  as  $P_v = P_{sat}(T_l) \exp \{ [v_l(P_l - P_{sat}(T_l))] / RT_l \}$  [15], where  $v_l$  is the specific volume of the liquid,  $P_{sat}(T_l)$  is the saturation pressure at  $T_l$ , and the liquid pressure  $P_l$  is approximated using the atmospheric pressure. Owing to the very small size of embryos, we assume that the temperature of liquid surrounding embryos is  $T_l \approx T$ , the surface temperature. If we denote  $J$  the generation rate per unit area of embryos having radius  $r_c$ ,  $J$  can be readily calculated using the thermodynamic conditions of the liquid [15, 21]. It follows that the duration to populate a unit area by bubbles of radius  $r_c$  is  $\tau_h = 1 / Jr_c^2$ . In Fig. 2a, we show the plots of  $2r_c$  and  $\log_{10}(\tau_h)$  versus  $T$  for acetone at the vicinity of Leidenfrost transition ( $T_L = 180^\circ\text{C}$  for acetone). The reduction in  $r_c$  indicates a decrease in thickness of the vapor layer at higher  $T$ . Remarkably, we also observe a sharp drop in  $\tau_h$ , implying that the required duration to generate a vapor layer becomes extremely small as  $T$  approaches the Leidenfrost transition. For instance, at  $T = 180^\circ\text{C}$ ,  $\tau_h = 1.6 \text{ ns}$ . This highlights the dominant role of the boiling process: a vapor layer is created immediately to separate the liquid from the surface if the liquid is sufficiently heated. However, we note that the boiling process takes away heat from the surface, causing its temperature to decrease, and as a result, the

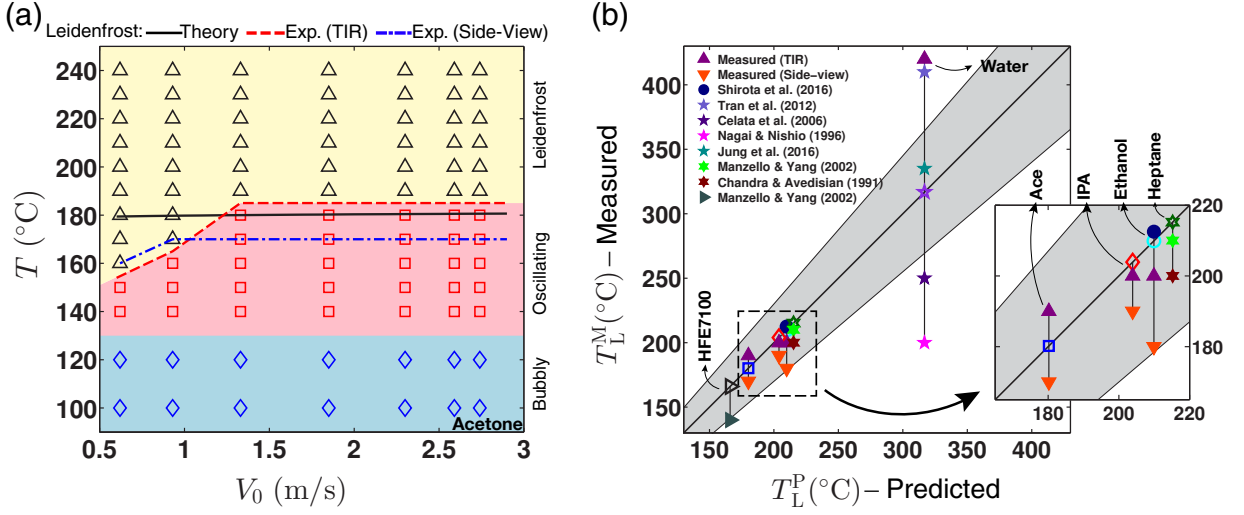


FIG. 3. (a) Phase diagram of characteristic boiling regimes of acetone. The solid line represents the theoretical prediction of the Leidenfrost transition (Eqn. 2); the dashed line and the dashed-dotted line respectively mark the Leidenfrost transition measured by TIR and side-view recordings. (b) Comparison between the Leidenfrost temperatures obtained from theory ( $T_L^P$ ) and those from experiments ( $T_L^M$ ). The open markers on the diagonal line indicate  $T_L^P$ . Upward solid triangles indicate  $T_L^M$  obtained from TIR; downward solid triangles indicate  $T_L^M$  from side-view recordings. All other solid markers are  $T_L^M$  from previous studies [10, 12, 13, 17–19]. The shaded area indicates  $\pm 15\%$  deviation from the theoretical values.

heterogeneous boiling process is forced to stop.

As soon as the heterogeneous boiling process stops, the liquid in neighbouring wetted areas merges and rewets the dry areas (Fig. 2b). From the contact line's motion, indicated in Fig. 2b, we measure rewetting velocity  $V_{re}$  for different liquids and impact velocity  $V_0$ . Generally,  $V_{re}$  is insensitive to  $V_0$  and increases with surface temperature  $T$  (see Fig. 2c and d). In order to understand this behavior, we note that a dry area resulted from heterogeneous boiling is covered by a vapor layer of thickness  $h \approx 2r_c$  (Fig. 2a, schematics). Since the tested liquids have small viscosities, the rewetting process is then driven by capillary pressure  $\sigma/2r_c$  and resisted only by inertia  $\rho_l V_{re}^2$  [22, 23]. Here, both the surface tension  $\sigma$  and density  $\rho_l$  are functions of surface temperature  $T$  [24]. Balancing the capillary pressure and inertia gives an estimate for the rewetting velocity

$$V_{re} \sim \left( \frac{\sigma}{2\rho_l r_c} \right)^{1/2} = \left( \frac{P_v - P_l}{4\rho_l F} \right)^{1/2}. \quad (1)$$

In Fig. 2c and d, we show several plots of  $V_{re}$  versus  $T$  for all tested liquids with impacting velocity  $V_0$  varying from  $0.6 \text{ m} \cdot \text{s}^{-1}$  to  $2.7 \text{ m} \cdot \text{s}^{-1}$ . We observe an excellent agreement with experimental results for acetone, ethanol, IPA, and an overestimate for water. We attribute possible drop in surface temperature during impact to the discrepancy in the case of water: due to its high latent heat and heat capacity compared to those of other liquids, the surface temperature in actuality may drop considerably during impact [18]. This causes an overestimation of the liquid temperature  $T_l$ , as well as the vapor pressure  $P_v(T_l)$ , leading to an overestimation of  $V_{re}$  (Eqn. 1). Nonetheless, these results not only suggest that the mea-

sured rewetting velocity is consistent with our theoretical arguments for the rewetting process, but also confirm that the vapor layer thickness is well described by the critical size of embryos. We conclude that the liquid-vapor dynamics in the oscillating boiling regime consist of two main processes: heterogeneous boiling followed by capillary-inertial rewetting.

We are now ready to derive an expression to determine the *dynamic* Leidenfrost transition, which marks the lower bound of the Leidenfrost regime for impacting droplets; the surface temperature at this transition is termed as *dynamic* Leidenfrost temperature  $T_L$ . We argue that at  $T = T_L$ , the upward speed of vapor generation must be comparable to the downward speed  $V_0$  of liquid. Since the heterogeneous boiling process generates a vapor layer of thickness  $h = 2r_c$  during the time  $\tau_h$ , the upward speed of vapor generation is  $V_v \sim 2r_c/\tau_h$ . Thus the dynamic Leidenfrost temperature  $T_L$  satisfies the condition

$$V_0 = \frac{2r_c(T_L)}{\tau_h(T_L)}. \quad (2)$$

This condition implicitly contains the dependence of  $T_L$  on  $V_0$  and the liquid properties, and we use it to determine the Leidenfrost transition for our tested liquids.

We calculate  $T_L$  for acetone using Eqn. 2 and show a plot of  $T_L$  vs.  $V_0$  (solid line, Fig. 3) together with a phase diagram consisting of three different characteristic behaviors: Leidenfrost, *oscillating* boiling, and bubbly boiling [10, 11] (Fig. 3). We identify and categorize these behaviors using TIR recordings of numerous impact experiments. We note that although both the oscillating boiling and bubbly boiling behaviors allow solid-liquid

contact, only the former exhibits high-frequency switching between the heterogeneous boiling and rewetting processes, while the boiling dynamics of the latter are much slower because of low surface temperature. In the phase diagram, the boundary separating the Leidenfrost and oscillating boiling regimes indicates the experimentally determined  $T_L$  (dashed line), which increases monotonically with  $V_0$  and reaches a plateau  $T_L = 190^\circ\text{C}$  at  $V_0 = 1.3\text{ m}\cdot\text{s}^{-1}$ , consistent with earlier studies [10, 12]. We also show the Leidenfrost temperature determined by *side-view* recordings (dashed-dotted line), a method incapable of directly detecting wetted areas during impact, but instead relying on ejection of small droplets as indication of wetted areas [10]. The discrepancy between values of  $T_L$  determined by side-view recordings and ones by TIR technique, although not significant, is therefore expected. Nevertheless, the plateaued values of  $T_L$  measured by both techniques are in remarkable agreement with the predicted value  $T_L = 180^\circ\text{C}$  using Eqn. 2, highlighting that the proposed prediction for  $T_L$  is valid for impacts at high velocity.

We emphasize that our prediction for  $T_L$  is not applicable for the case of low impact velocity, e.g.,  $V_0 \leq 1.3\text{ m}\cdot\text{s}^{-1}$ , where liquid-solid separation results from the viscous stress induced by air/vapor flows under impacting droplets. The viscous stress is responsible for phenomena such as dimple formation [10, 25], bubble entrapment [26], or even bouncing from unheated surfaces for droplets at small impact velocity [9]. We note that for  $V_0 \leq 1.3\text{ m}\cdot\text{s}^{-1}$ , the compressible effect is negligible and the thickness of the air/vapor film under a droplet decreases with increasing  $V_0$  [25]. The increase in  $T_L$  with  $V_0$  is expected to sustain the liquid-solid separation. Thus the deviation of the predicted values of  $T_L$  from the experimental ones at low impact velocity reveals the region where the viscous stress caused by the air/vapor flows becomes the dominant mechanism for separation.

In Fig. 3b, we show a plot comparing the experimental Leidenfrost temperature ( $T_L^M$ ) to the predicted one ( $T_L^P$ ) for six different liquids having broadly different thermal and physical properties. For each liquid, we use the plateaued value of  $T_L$  (shown in Fig. 3b) as the experimentally measured one. The plot also consists of numerous experimental datasets from previous studies in which measurements of the dynamic Leidenfrost temperature were reported; most of them utilized the side-view technique to determine  $T_L$ . Except for water, we observe that all the experimental values of  $T_L$  are consistent, within 15% deviation, with the predicted ones; typically the TIR measured values are closer to theory than those obtained by the side-view technique. We note that while the surface temperature is assumed constant in our simplified theory, it fluctuates considerably in reality [12, 27, 28] as a result of two competing heat transfer processes: one from the solid surface to the liquid, and the other from the solid bulk to the surface. In addition,

variations in surface roughness and impact velocity may contribute to discrepancy between  $T_L^M$  and  $T_L^P$ . In the case of water, which has exceptionally high heat capacity and latent heat compared to other tested liquids (Table I), we expect a more severe drop in surface temperature, which may be the main cause of the vastly disparate reported values for  $T_L^M$  (from  $200^\circ\text{C}$  to  $410^\circ\text{C}$ ). The reduction in surface temperature, however, implies that the theory underestimates  $r_c$  and subsequently overestimates  $V_{re}$ , consistent with the result shown in Fig. 2d for water. In other words, the prediction of  $T_L$  for water is missing a prefactor to account for the substantial drop in surface temperature. A detailed analytical prediction of  $T_L$  for water, therefore, must be derived on the ground of non-negligible fluctuation in surface temperature and merits further investigation.

From our experimental measurements and analysis of  $T_L$ , we infer that there are two fundamentally different mechanisms for Leidenfrost transition at two extremes of velocity. At low impact velocity, the separation mechanism is mainly associated the viscous stress induced in the air/vapor flows. By contrast, at high impact velocity, the mechanism for Leidenfrost transition is dictated by the heterogeneous boiling process, i.e., the kinetic limit of superheat at the solid-liquid interface. This explains the asymptotic behavior of the Leidenfrost transition at high impact velocity. The heterogeneous boiling process also causes the oscillating boiling behavior, i.e., high-frequency fluctuation of the wetted area due to alternative domination of either heterogeneous boiling or rewetting over the other. The transition to Leidenfrost regime, therefore, reduces to the sustaining capability of the heterogeneous boiling process. For practical boiling applications at high temperatures, a direct implication from our theory is that in order to avoid the boiling crisis, the properties of both the liquid and the boiling surface should be selected to obtain high rewetting velocity and subsequently to sustain heterogeneous boiling. Furthermore, the role of capillary-inertial rewetting in the transition to boiling crisis on smooth surfaces can be further extended to design rough surfaces used in boiling. We conclude by highlighting that our findings offer a theoretical framework to treat the Leidenfrost transition, a crucial step toward achieving complete control of the Leidenfrost effect.

## ACKNOWLEDGMENTS

We thank H. Kellay and P. Chakraborty for helpful discussions. This work was funded by Nanyang Technological University and A\*STAR, Singapore. M. Khavari acknowledges SINGA scholarship from A\*STAR.



---

\* Corresponding author: ttran@ntu.edu.sg

- [1] G. Berthoud, *Ann. Rev. of Fluid Mech.* **32**, 573 (2000); J. Kim, *Int. J. Heat Fluid Fl.* **28**, 753 (2007).
- [2] H. Linke, B. Alemán, L. Melling, M. Taormina, M. Francis, C. Dow-Hygelund, V. Narayanan, R. Taylor, and A. Stout, *Phys. Rev. Lett.* **96**, 154502 (2006); I. U. Vakarelski, J. O. Marston, D. Y. Chan, and S. T. Thoroddsen, *ibid.* **106**, 214501 (2011); I. U. Vakarelski, N. A. Patankar, J. O. Marston, D. Y. Chan, and S. T. Thoroddsen, *Nature* **489**, 274 (2012).
- [3] J. Leidenfrost, Duisburg (1756), Translation: On the fixation of water in diverse fire, *Int. J. Heat Mass Trans.* **9**, 1153-1166 (1966).
- [4] J. D. Bernardin and I. Mudawar, *Int. J. Heat Mass Trans.* **38**, 863 (1995); *J. Heat Transfer* **126**, 272 (2004); G. Liang and I. Mudawar, *Int. J. Heat Mass Trans.* **106**, 103 (2017).
- [5] B. Gottfried, C. Lee, and K. Bell, *Int. J. Heat Mass Trans.* **9**, 1167 (1966).
- [6] A.-L. Biance, C. Clanet, and D. Quéré, *Phys. Fluids* **15**, 1632 (2003).
- [7] J. Bernardin and I. Mudawar, *J. Heat Transfer* **121**, 894 (1999).
- [8] M. Rein, *Drop-surface interactions*, Vol. 456 (Springer, Wien, New York, 2002).
- [9] J. de Ruiter, R. Lagraauw, D. van den Ende, and F. Mugele, *Nature Phys.* **11**, 48 (2015).
- [10] T. Tran, H. J. Staat, A. Prosperetti, C. Sun, and D. Lohse, *Phys. Rev. Lett.* **108**, 036101 (2012).
- [11] M. Khavari, C. Sun, D. Lohse, and T. Tran, *Soft Matter* **11**, 3298 (2015).
- [12] M. Shirota, M. A. van Limbeek, C. Sun, A. Prosperetti, and D. Lohse, *Phys. Rev. Lett.* **116**, 064501 (2016).
- [13] N. Nagai and S. Nishio, *Exp. Therm. Fluid Sci.* **12**, 373 (1996).
- [14] J. M. Kolinski, S. M. Rubinstein, S. Mandre, M. P. Brenner, D. A. Weitz, and L. Mahadevan, *Phys. Rev. Lett.* **108**, 074503 (2012).
- [15] V. P. Carey, *Liquid-vapor phase-change phenomena* (Hemisphere, New York, NY, 1992).
- [16] R. Cole, *Adv. Heat Transfer* **10**, 85 (1974).
- [17] G. Celata, M. Cumo, A. Mariani, and G. Zummo, *Heat Mass Transf.* **42**, 885 (2006).
- [18] J. Jung, S. Jeong, and H. Kim, *Int. J. Heat Mass Trans.* **92**, 774 (2016).
- [19] S. L. Manzello and J. C. Yang, *Int. J. Heat Mass Trans.* **45**, 3961 (2002); S. Chandra and C. Avedisian, *Proc. R. Soc. London, Ser. A* **432**, 13 (1991).
- [20] The factor  $F = 0.5 + 0.75 \cos \theta - 0.25 \cos^3 \theta$  is the correction factor that accounts for partially wettable liquids with contact angle  $\theta$ .
- [21] The embryo formation rate  $J$  relates to liquid properties and boiling conditions as [15]  $J = \Gamma_1 \Gamma_2 \Gamma_3$ , where  $\Gamma_1 = \rho_{N,l}^{2/3} (1 + \cos \theta) / 2F$ ,  $\Gamma_2 = [3F \sigma_{lv} / (\pi m)]^{1/2}$ ,  $\Gamma_3 = \exp\{-16\pi F \sigma_{lv}^3 / \{3k_B T_l [\eta P_{sat}(T_l) - P_l]^2\}\}$ , and  $\eta = \exp\{v_l [P_l - P_{sat}(T_l)] / (RT_l)\}$ . Here  $\rho_{N,l} = N_A / (v_l \bar{M})$  is the number density of liquid molecules per unit volume,  $m = \bar{M} / N_A$  the mass of one molecule,  $\bar{M}$  the molecular mass in  $\text{kg} \cdot \text{kmol}^{-1}$ ,  $N_A = 6.02 \times 10^{26} \text{ kmol}^{-1}$  the Avogadro constant,  $k_B = 1.38 \times 10^{-23} \text{ J} \cdot \text{K}^{-1}$  the Boltzmann constant,  $R = \bar{R} / \bar{M}$  the specific gas constant in  $\text{J} \cdot \text{kg}^{-1} \cdot \text{K}^{-1}$ , and  $\bar{R} = 8314.4 \text{ J} \cdot \text{K}^{-1} \cdot \text{kmol}^{-1}$  the universal gas constant.
- [22] M. Wu, T. Cubaud, and C.-M. Ho, *Physics of Fluids* **16**, L51 (2004).
- [23] K. G. Winkels, J. H. Weijs, A. Eddi, and J. H. Snoeijer, *Phys. Rev. E* **85**, 055301 (2012).
- [24] Since the surface tension  $\sigma$ , specific volume  $v_l$ , and saturation pressure  $P_{sat}$  of each liquid depend strongly on the liquid temperature  $T_l$ , we interpolate their temperature-dependent values from the reported data for the tested liquids, including acetone, ethanol, water, and heptane [29], IPA [30, 31] and HFE7100 [32].
- [25] E. Li and S. T. Thoroddsen, *J. Fluid Mech.* **780**, 636 (2015).
- [26] R. C. van der Veen, T. Tran, D. Lohse, and C. Sun, *Phys. Rev. E* **85**, 026315 (2012); W. Bouwhuis, R. C. van der Veen, T. Tran, D. L. Keij, K. G. Winkels, I. R. Peters, D. van der Meer, C. Sun, J. H. Snoeijer, and D. Lohse, *Phys. Rev. Lett.* **109**, 264501 (2012).
- [27] M. Seki, H. Kawamura, and K. Sanokawa, *J. Heat Transfer*, 1213 (1962).
- [28] M. A. van Limbeek, M. Shirota, P. Sleutel, C. Sun, A. Prosperetti, and D. Lohse, *Int. J. Heat Mass Trans.* **97**, 101 (2016).
- [29] A. Faghri and Y. Zhang, *Transport phenomena in multi-phase systems* (Academic Press, 2006).
- [30] D. Ambrose, J. Counsell, I. Lawrenson, and G. Lewis, *J. Chem. Thermodyn.* **10**, 1033 (1978).
- [31] B. C. Hoke Jr and J. C. Chen, *J. Chem. Eng. Data* **36**, 322 (1991).
- [32] M. H. Rausch, L. Kretschmer, S. Will, A. Leipertz, and A. P. Froba, *J. Chem. Eng. Data* **60**, 3759 (2015).
- [33] D. R. Lide, *CRC handbook of chemistry and physics* (CRC Press, 2004).